TE-TM dynamics in a semiconductor laser subject to polarization-rotated optical feedback

T. Heil,* A. Uchida,† P. Davis, and T. Aida‡
ATR Adaptive Communications Research Laboratories, 2-2-2 Hikaridai, Seika-cho, Soraku-gun, Kyoto 619-0288, Japan
(Received 12 August 2002; published 25 September 2003)

We present a comprehensive experimental characterization of the dynamics of semiconductor lasers subject to polarization-rotated optical feedback. We find oscillatory instabilities appearing for large feedback levels and disappearing at large injection currents, which we classify in contrast to the well-known conventional optical-feedback-induced dynamics. In addition, we compare our experiments to theoretical results of a single-mode model assuming incoherence of the optical feedback, and we identify differences concerning the average power of the laser. Hence, we develop an alternative model accounting for both polarizations, where the emission of the dominant TE mode is injected with delay into the TM mode of the laser. Numerical simulations using this model show good qualitative agreement with our experimental results, correctly reproducing the parameter dependences of the dynamics. Finally, we discuss the application of polarization-rotated-feedback induced instabilities in chaotic carrier communication systems.

DOI: 10.1103/PhysRevA.68.033811 PACS number(s): 42.65.Sf, 42.55.Px, 05.45.Xt

I. INTRODUCTION

Communication schemes using chaotic carrier signals have great potential for secure communication [1]. Realizing high-speed synchronized chaos is a major challenge in the development of these novel schemes. Demonstrations of broadband synchronized chaos in the GHz range have been given using fiber laser systems [2,3] and semiconductor laser (SL) systems [4–6]. In particular, SLs subject to delayed optical feedback exhibit a particularly high potential for use in practical applications due to their very fast and high-dimensional chaotic dynamics, cost efficiency, simple configuration, and compatibility with already existing optical communication systems. However, the use of chaotic carrier signals generated in SLs using coherent optical feedback also requires coherent optical injection into the receiver SL system to achieve synchronization, though it is very difficult to guarantee such a coherent coupling into the receiver system after transmission of a chaotic carrier over a long distance through optical fiber. Therefore, the realization of high-speed synchronized chaos, which does not depend on coherent injection to the receiver laser, is highly desirable for practical applications. The use of SLs subject to incoherent optical feedback directly acting only on the carrier density in the laser rather than the optical field could be a way to fulfill these requirements. SLs with incoherent optical feedback have previously been studied theoretically using rate equation models [7–10], and polarization-rotated feedback has been proposed [11–13] as a method to realize this theoretical concept experimentally. Polarization-rotated optical feedback has already been used for frequency stabilization of SL emission [14,15], and an experiment on the dynamics of a SL with polarization-rotated feedback has been performed recently [16]. However, a detailed characterization and investigation of the dynamics of SLs subject to polarization-rotated feedback is still lacking. In particular, the question of how polarization-rotated feedback corresponds to incoherent optical feedback in the sense of Refs. [7–13] remains unclear.

In this paper, we present a comprehensive characterization of the dynamics of SLs subject to polarization-rotated optical feedback. Our experimental and numerical investigations are strongly motivated by possible advantages of chaos generated by SLs subject to polarization-rotated optical feedback for applications as chaotic carriers in future communication systems. In the experimental section, Sec. II, we characterize the dynamics of the system for different SL structures, showing the dependence on two key parameters, namely feedback level and injection current. In particular, we provide a full overview of the intensity dynamics combined with an analysis of the corresponding optical spectra. A careful comparison of our experimental results with previous theoretical results reveals some inconsistencies. Accordingly, in Sec. III, we extend the previous rate equation models in order to fully account for the polarization-rotated optical feedback without *a priori* assuming an incoherent feedback effect. Numerical simulations of the feedback level and injection current dependence of the dynamics of the system using the new model are in good qualitative agreement with our experimental results. Finally, in Sec. IV, we discuss our results and present some conclusions.

II. EXPERIMENTS

A. Setup

Figure 1 shows our experimental setup. We use two different types of SLs: first, a single-mode distributed-feedback (DFB) laser (NEL: NLK1555CCA) with an operation wavelength of 1537 nm, and a threshold current of 9.8 mA; second, a multimode Fabry-Perot (FP) laser (Anritsu SD3F513T) emitting around 1460 nm with a threshold cur-

*Present address: Carl Zeiss Semiconductor Manufacturing Technologies AG, Carl Zeiss Strasse 22, 73447 Oberkochen, Germany.
†Present address: Institute for Research in Electronics and Applied Physics, University of Maryland, College Park, MD, 20742, USA.
‡Present address: NHK Science and Technical Research Laboratories, 1-10-11 Kinuta, Setagaya-ku, Tokyo 157-8510, Japan.

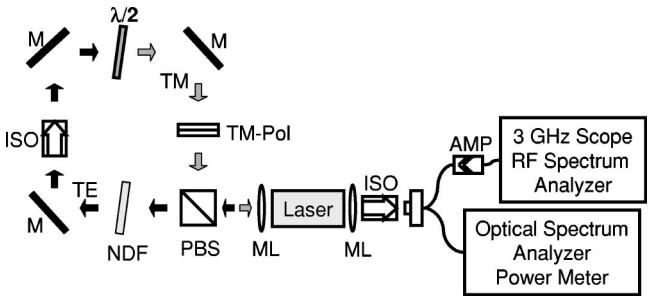

FIG. 1. Experimental setup for observation of polarization-rotated dynamics. The SL oscillating mainly in the TE mode is subject to delayed polarization-rotated optical feedback injected into the TM mode of the laser. Amp, amplifier; ISO, optical isolator; M, mirror; ML, microscopic lens; NDF, ND filter; PBS, polarization beam splitter; TE, TE-polarization mode; TM, TM-polarization mode; TM-Pol, polarizer along TM direction; λ/2, half-wave plate.

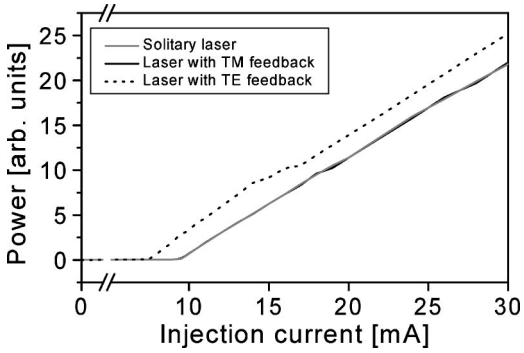

FIG. 2. Power-injection current characteristics for the solitary DFB laser (the gray solid curve), the laser with polarization-rotated TM-mode feedback (the black solid curve), and the laser with conventional TE-mode feedback (the dotted curve), obtained in experiment.

rent of 25 mA. At two times threshold, both the solitary DFB laser and the solitary FP laser exhibit single transverse-electric (TE) mode emission with transverse-magnetic (TM) mode suppression ratios of 1000 and 750, respectively. Both lasers exhibit an AR coating of 0.1% on one of their facets. The lasers are driven by a low-noise current source (Newport: Model 8008) and temperature-stabilized with 0.01 K accuracy.

The delayed optical feedback is provided by an external optical loop circuit which polarizes the laser beam, rotates this polarization by 90°, and reinjects this polarization-rotated beam back into the laser. The delay time is given by the round-trip time of the light in the loop, and amounts to $\tau = 7.4$ ns, corresponding to a round-trip frequency of $\nu_{\mathrm{rt}} = \tau^{-1} = 0.135$ GHz. The individual optical components are the following. An optical isolator (ISO) is used to achieve one-way loop propagation with isolation of -60 dB. A half-wave plate (λ/2) rotates the polarization direction of the laser beam by 90° from TE mode to TM mode, and a polarizer (TM-Pol) is used to ensure only the TM mode returns to the laser. The feedback loop is formed by mirrors (M) and a polarization beam splitter (PBS), which feeds the outgoing TE beam into the loop and feeds the returning TM beam back into the laser. A neutral density filter (NDF) controls the strength of optical feedback.

The AR-coated facet of the lasers is used to provide the optical feedback, and the light from the uncoated facet is used for detection. The optical spectrum is measured with an optical spectrum analyzer (Anritsu MS9710C) with a resolution of 0.05 nm. The dynamical behavior of the intensity is detected with a 6 GHz photodiode (New Focus 1514-LF) and analyzed with a radiofrequency spectrum analyzer (Advantest R3267, 9 GHz bandwidth) and a fast digital oscilloscope (Tektronix TDS694C, 3-GHz bandwidth).

B. Results

In this section, we first characterize the dynamics of a SL subject to polarization-rotated feedback using the DFB laser. Then, we investigate the effect of multimode emission by comparing the DFB laser results to those obtained with the FP laser. Finally, we present a brief discussion of the obtained results connecting the experimental and theoretical part of this paper.

As a first step, we measure the characteristics of the output power as a function of injection current (P-I curve) as shown in Fig. 2. We plot the P-I curves for the solitary DFB laser (the gray solid curve in Fig. 2), the laser with polarization-rotated TM-mode feedback (the black solid curve), and the laser with conventional TE-mode feedback (the dotted curve). All curves are recorded for a similar level of optical feedback. The plots show the average power, i.e., the dc component when the intensity is oscillating. The P-I curve for the TE-mode feedback is typical for coherent optical feedback, see, e.g., [17]. There is a typical threshold reduction of 20%. The kink in the P-I curve marks the onset of chaotic fluctuations induced by the coherent optical feedback. However, for the TM-mode feedback, the P-I curve is similar to that for the solitary laser. Specifically, there is no threshold reduction and almost no change of slope. Thus, the time-averaged intensity of the laser is almost unaffected by the polarization-rotated TM-mode feedback. However, observing the temporal waveforms of the intensity, we find characteristic TM-feedback-induced instabilities.

First, we investigate the injection current dependence of these feedback-induced instabilities. Figure 3 shows the temporal waveforms of the DFB laser with polarization-rotated feedback at various injection currents, and Fig. 4 displays the corresponding rf spectra. For low injection currents of 1.15 times the solitary laser threshold $J_{\mathrm{th,sol}}$, we observe the small-amplitude instabilities shown in Fig. 3(a). The corresponding rf spectrum depicted in Fig. 4(a) shows a series of equidistant peaks separated by the round-trip frequency ν_{rt}. The amplitudes of these peaks exhibit a characteristic envelope with a maximum approximately at the relaxation oscillation frequency. As the current is increased, the amplitude of the oscillations increases. Figure 3(b) shows a typical example observed for $1.25J_{\mathrm{th,sol}}$. The instabilities appear to be weakly chaotic oscillations which are close to quasiperiodicity. Figure 4(b) demonstrates that the instabilities are dominated by two basic frequency components: a low-frequency component which is the round-trip frequency (inverse delay

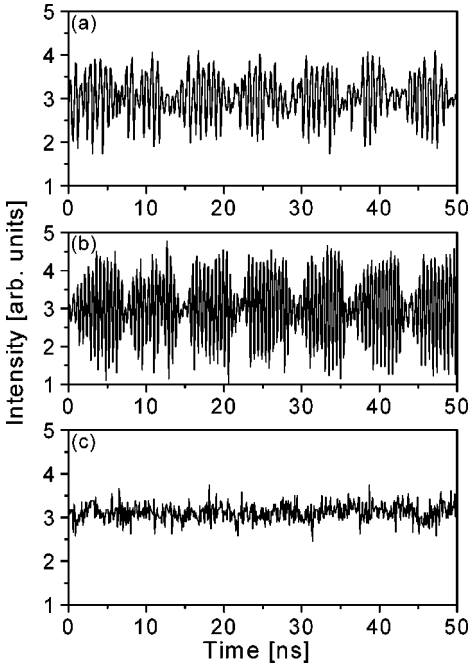

FIG. 3. Temporal waveforms of a DFB SL subject to polarization-rotated optical feedback at various injection currents. (a) $J=1.15J_{\mathrm{th,sol}}$, (b) $J=1.25J_{\mathrm{th,sol}}$, (c) $J=2.0J_{\mathrm{th,sol}}$.

time) and a high-frequency component near the relaxation oscillation frequency. Interestingly, the positions of the peak associated with the round-trip frequency do not shift with increasing injection current. This is in contrast to the dynamics of SLs with coherent TE feedback, where a significant shift and broadening of these peaks occurs for increasing injection current. Finally, as the current ratio is increased further, the amplitude of the intensity oscillations decreases again, as shown in Fig. 3(c), which depicts the intensity dynamics for $2.0J_{\mathrm{th,sol}}$, and in Fig. 4(c) showing the corresponding rf spectra. The amplitude of the peaks is substantially reduced for large injection currents. Thus, we find a characteristic behavior of dependence of the amplitude of the TM-feedback-induced instabilities on the injection current. The amplitudes are largest for $1.3J_{\mathrm{th,sol}}$, whereas the instabilities totally disappear for injection currents over $2.5J_{\mathrm{th,sol}}$, where we observe stable steady-state output with flat rf spectra. There are small kinks around $1.7J_{\mathrm{th,sol}}$ and $2.6J_{\mathrm{th,sol}}$ on the *P-I* curve for TM-mode feedback shown in Fig. 2. However, unlike the case of coherent feedback, we do not observe significant changes in dynamical behaviors at these small kinks.

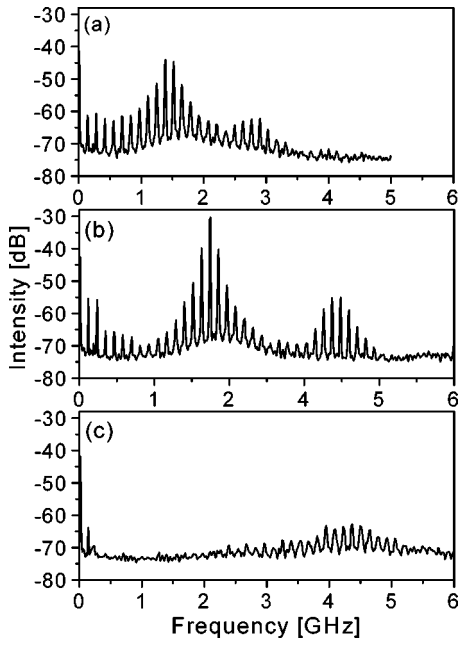

FIG. 4. rf spectra corresponding to Fig. 3.

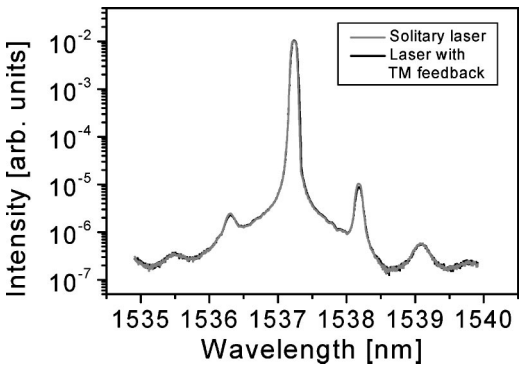

FIG. 5. Optical spectra for the solitary DFB laser (the gray solid curve) and the laser with polarization-rotated TM-mode feedback corresponding to Fig. 3(b) (the black solid curve).

Figure 5 compares the optical spectrum of the DFB laser with polarization-rotated TM-mode feedback (the black solid curve) to the solitary laser optical spectrum (the gray solid curve). The experimental conditions correspond to Fig. 3(b). Figure 5 demonstrates that the change in the optical spectrum due to the polarization-rotated TM-mode feedback is almost unnoticeable at this resolution. In particular, the peak in the optical spectrum for TM-mode feedback is not broadened as much as for the coherent TE-mode feedback, where a substantial broadening of the optical linewidth is observed. This indicates a less pronounced spectral dynamics for polarization-rotated feedback.

Another basic parameter in delayed feedback systems is the feedback strength. We control the optical feedback in our experiment using a neutral density filter. We find that for a decreasing level of optical feedback, the amplitudes of the TM-feedback-induced instabilities continuously reduce. Furthermore, we do not observe qualitative changes in the dynamics while the amplitudes decrease. When the feedback level is reduced to as much as 5% of that present in Fig. 3, the instabilities disappear and the rf spectrum flattens out. We note that for this level of coherent TE-mode feedback, we observe large-amplitude instabilities in association with a broad rf spectrum and a broadened optical spectrum. Thus, our experiment clearly demonstrates that much stronger optical feedback is required to induce instabilities in the case of TM-mode feedback. This clearly distinguishes the polarization-rotated TM-mode feedback from the coherent TE-mode feedback where already very small amounts of op-

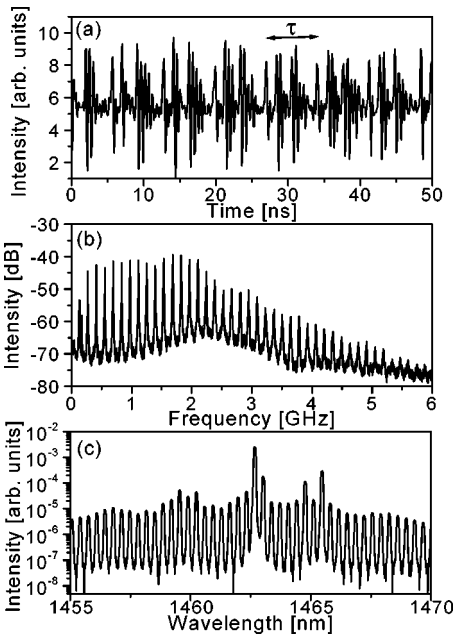

FIG. 6. Dynamics in a Fabry-Perot SL subject to polarization-rotated feedback. (a) Temporal waveform, (b) rf spectrum, and (c) optical spectrum. The injection current is $J=1.36J_{\mathrm{th,sol}}$.

tical feedback are sufficient to induce instabilities in the laser.

In order to investigate the influence of the type of laser structure on the characteristics of the TM-mode-feedback-induced instabilities, we exchanged the DFB laser structure for a Fabry-Perot type SL. These are the two most popular laser types of SL structures. The major difference between DFB and FP structures is the number of longitudinal modes on which the laser operates. Recently, there has been an intense discussion about the significance of the number of longitudinal modes for the dynamics of SLs subject to coherent TE-mode feedback [18–20]. In order to study this question also for the case of polarization-rotated TM-mode feedback, we repeat the DFB laser measurements reported above for the FP laser. For a similar feedback level, the *P-I* curve of the FP laser oscillating in multiple longitudinal modes shows a behavior similar to the DFB laser, i.e., no threshold reduction and only very slightly (2%) increasing power. The corresponding intensity dynamics and optical spectra are characterized in Fig. 6. The intensity time series depicted in Fig. 6(a) appears to be more chaotic than that of the DFB laser. Nevertheless, strong correlations associated with the delay time are present, and the temporal dynamics are still close to quasiperiodicity. This is clear from the rf spectrum depicted in Fig. 6(b), showing the characteristic series of peaks separated by the inverse delay time and an envelope with a hump around the relaxation oscillation frequency. Accordingly, the rf spectra of the FP laser and the DFB laser exhibit similar qualitative features, though the individual peaks for the FP laser case are slightly more broadened. The optical spectrum of the FP laser subject to polarization-rotated TM-mode feedback depicted in Fig. 6(c) showing a series of longitudinal modes is similar to that of the solitary FP laser.

Concerning the parameter dependences, we observe in both laser types qualitatively the same behavior. Using the FP laser, the same high levels of optical feedback are required in order to obtain polarization-rotated-feedback-induced instabilities. Moreover, increasing the injection current leads to the characteristic instabilities already described for the DFB laser. Also, for even higher pumping currents over $2.0J_{\mathrm{th,sol}}$, the instabilities disappear again. To sum up, we observe some minor modifications of the dynamics of a SL subject to polarization-rotated feedback which may be linked to the multimode emission of the laser. However, the basic qualitative features of the dynamics that we observed remain the same, confirming that similar dynamics can be observed in both single-mode and multimode SLs.

Table I summarizes the experimental results presented in this section. In particular, we compare and contrast our new results characterizing the dynamics of a SL with polarization-rotated TM-mode feedback with the already well known characteristics of the instabilities caused by coherent TE-mode feedback.

One motivation for the experiments presented in this section is to investigate the possibility of generating high-speed synchronized chaos that does not depend on coherent injection into the receiver laser. As already mentioned, the concept of incoherent optical feedback has been considered for this purpose [11–13]. Incoherent optical feedback is present if the feedback only acts on the carrier density, but leaves the complex electrical field amplitude unaffected [7–10]. The question whether polarization-rotated optical feedback is an effective method to realize such incoherent optical feedback

TABLE I. Dynamics of SLs subject to delayed optical feedback. Comparison of polarization-rotated TM-mode feedback versus coherent TE-mode feedback.

	Polarization-rotated TM-mode feedback	Coherent TE-mode feedback
Threshold reduction	No	Yes
Slope of *P-I* curve	Unchanged	Changed
Dynamics	Weakly chaotic, almost quasiperiodic	Chaotic, typ. high dimensional
Amplitude of instabilities	Rather small	Large
Onset of instabilities	Strong feedback required	Weak feedback sufficient
Strong pumping	Instabilities disappear	Instabilities persist
Peaks in rf spectrum	Position constant	Position shifts

TABLE II. Parameter values for semiconductor lasers used in our calculations.

Symbol	Parameter	Value
G_{TE}	Gain coefficient for TE mode	1.374×10^{-12} m^3 s^{-1}
G_{TM}	Gain coefficient for TM mode	1.154×10^{-12} m^3 s^{-1}
N_0	Carrier density at transparency	1.400×10^{24} m^{-3}
γ_{inj}	Injection coefficient	7.000×10^{10} s^{-1}
$\gamma_{p,\mathrm{TE}}$	Inverse of photon lifetime for TE mode	8.913×10^{11} s^{-1}
$\gamma_{p,\mathrm{TM}}$	Inverse of photon lifetime for TM mode	8.913×10^{11} s^{-1}
γ_{s}	Inverse of carrier lifetime	4.902×10^{8} s^{-1}
τ	Propagation time of the external loop	6.67×10^{-9} s
α	Linewidth enhancement factor	3.0
J	Injection current density	$1.4J_{\mathrm{th,sol}}$
$J_{\mathrm{th,sol}}$	Threshold of injection current density	1.004×10^{33} m^{-3} s^{-1}
λ	Wavelength of laser	1537 nm

experimentally was still to be answered. In a previous experiment, a reduction in laser power due to the polarization-rotated optical feedback has been observed [16]. This reduction has been predicted in the single-mode model of incoherent feedback [7–10]. According to this model, the slope of the *P-I* curve of the SL should decrease by $\eta/(1+\eta)$ due to the incoherent optical feedback, where η is the feedback power ratio.

However, as summarized in Table I, the results of our systematic investigations of SLs subject to polarization-rotated optical feedback are not in every point consistent with the single-mode incoherent feedback model. While the quasiperiodic nature of the oscillations obtained for large optical feedback levels and moderate current injection level have similarities with those observed in previous models for delayed incoherent feedback using polarization-rotated feedback [7–10] and optoelectronic feedback [21–23], and the absence of threshold reduction is in agreement with the single-mode incoherent feedback model, the unchanged slope of the *P-I* curve represents a discrepancy. This last result indicates that we need to modify the single-mode incoherent feedback model to match our experimental system. Accordingly, we have extended the incoherent feedback model by accounting for both polarizations present in the laser. Our extended model allows us to directly investigate the effect of polarization-rotated feedback without assuming incoherence of the optical feedback beforehand. The following section provides a detailed description of this new model.

III. NUMERICAL CALCULATIONS

Model

In this section, we present a numerical model which describes behavior similar to that seen in our experiments. We use a two-mode dynamical model, allowing for the dynamics of the TM mode as well as the TE mode in the laser. A similar model including nonlinear gain terms has previously been used to describe TE-TM dynamics in SLs [24–26]. The rate equations for TE and TM modes are described as follows:

$$\frac{dE_{\mathrm{TE}}(t)}{dt}=\frac{1}{2}\{G_{\mathrm{TE}}[N(t)-N_0]-\gamma_{p,\mathrm{TE}}\}E_{\mathrm{TE}}(t), \tag{3.1}$$

$$\frac{d\Phi_{\mathrm{TE}}(t)}{dt}=\frac{\alpha}{2}\{G_{\mathrm{TE}}[N(t)-N_0]-\gamma_{p,\mathrm{TE}}\}, \tag{3.2}$$

$$\frac{dE_{\mathrm{TM}}(t)}{dt}=\frac{1}{2}\{G_{\mathrm{TM}}[N(t)-N_0]-\gamma_{p,\mathrm{TM}}\}E_{\mathrm{TM}}(t)+\gamma_{\mathrm{inj}}E_{\mathrm{TE}}(t-\tau)\cos\Delta(t), \tag{3.3}$$

$$\frac{d\Phi_{\mathrm{TM}}(t)}{dt}=\frac{\alpha}{2}\{G_{\mathrm{TM}}[N(t)-N_0]-\gamma_{p,\mathrm{TM}}\}-\gamma_{\mathrm{inj}}\frac{E_{\mathrm{TE}}(t-\tau)}{E_{\mathrm{TM}}(t)}\sin\Delta(t), \tag{3.4}$$

$$\frac{dN(t)}{dt}=J-\gamma_{\mathrm{s}}N(t)-[N(t)-N_0]\times\{G_{\mathrm{TE}}|E_{\mathrm{TE}}(t)|^2+G_{\mathrm{TM}}|E_{\mathrm{TM}}(t)|^2\}, \tag{3.5}$$

$$\Delta(t)=\omega_0\tau+\Phi_{\mathrm{TM}}(t)-\Phi_{\mathrm{TE}}(t-\tau), \tag{3.6}$$

where E and Φ are the electrical amplitude and the phase, N is the carrier density, and Δ is the phase difference. The subscripts TE and TM indicate the TE and TM modes, respectively. G is the gain coefficient and N_0 is the carrier density at the transparency. γ_{inj} is the injection coefficient, γ_p is the inverse of the photon lifetime, γ_s is the inverse of the carrier lifetime, τ is the propagation time of the external loop, α is the linewidth enhancement factor, J is the injection current density, and $J_{\mathrm{th,sol}}=\gamma_s(N_0+\gamma_{p,\mathrm{TE}}/G_{\mathrm{TE}})$ is the threshold of the injection current density. ω_0 is the angular frequency, and $\lambda=2\pi c/\omega_0$ is the wavelength. We ignore the small contributions from nonlinear gain suppression and spontaneous emission. Some typical parameters are given in Table II. In our calculation, the Langevin noise terms are ignored for the sake of simplicity. We also neglect the non-

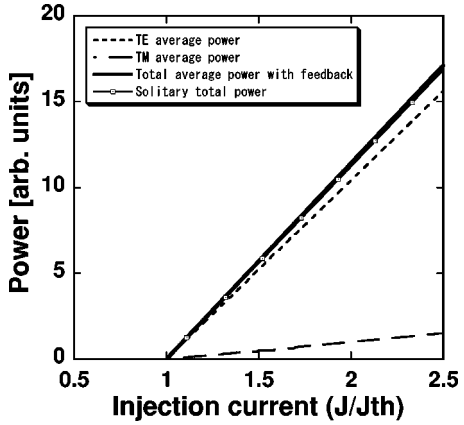

FIG. 7. Power-injection current (P-I) characteristics calculated from our model. Black thick line, total output of the laser with TM feedback; solid line with squares, solitary laser output; dotted line, TE-component output of the laser with TM-mode feedback; dashed line, TM-component output of the laser with TM feedback.

linear gain. We numerically integrate Eqs. (3.1)–(3.6) by employing the Runge-Kutta-Gill method.

There are two considerations in matching parameter values which give behavior similar to that observed in experiments, namely matching the onset of oscillations and matching the P-I curve for the dependence of average power on injection current ratio. The total power $P_{\mathrm{total}}=\langle|E_{\mathrm{TE}}|^2+|E_{\mathrm{TM}}|^2\rangle$ (the anglular brackets denote time averaging) can be analytically described in our model as follows:

$$P_{\mathrm{total}}=\frac{1+P_{\mathrm{ratio}}}{G_{\mathrm{ratio}}+P_{\mathrm{ratio}}}P_{\mathrm{sol}}, \tag{3.7}$$

where P_{sol} is the power of the solitary laser, $G_{\mathrm{ratio}}=G_{\mathrm{TM}}/G_{\mathrm{TE}}$ is the gain ratio of TM mode to TE mode, and $P_{\mathrm{ratio}}=P_{\mathrm{TE}}/P_{\mathrm{TM}}$ is the power ratio of TE mode to TM mode. P_{ratio} is described as follows from the steady-state solution:

$$P_{\mathrm{ratio}}=\frac{1+\alpha^2}{4}\left(\frac{\gamma_{p,\mathrm{TE}}}{\gamma_{\mathrm{inj}}}\right)^2\left(\frac{\gamma_{p,\mathrm{TM}}}{\gamma_{p,\mathrm{TE}}}-\frac{G_{\mathrm{TM}}}{G_{\mathrm{TE}}}\right)^2. \tag{3.8}$$

We note that in this model the power ratio P_{ratio} is a key parameter for the onset of self-oscillations, because the coupling term in the carrier equation of Eq. (3.5) depends on the power ratio. Specifically, once the known laser parameters are fixed, we found that the onset of oscillations similar to the experiments can be obtained for a power ratio of around 10. Then by choosing an appropriate value of the gain ratio, we obtained a match also of the P-I curve. Specifically, if we set $P_{\mathrm{ratio}}=10.4$ and $G_{\mathrm{ratio}}=0.84$ by using the parameter values shown in Table II, then the power ratio is obtained as $P_{\mathrm{total}}=1.014P_{\mathrm{sol}}$, and so the total power is almost the same as the power of the solitary laser. Figure 7 shows the P-I curves for the total output of the solitary laser (the solid line with squares), total output of the laser with TM-mode feedback (the black thick line), the TE-component output of the laser with TM feedback (the dotted line), and the TM-component output of the laser with TM feedback (the dashed line), obtained from our numerical calculations. Note that no

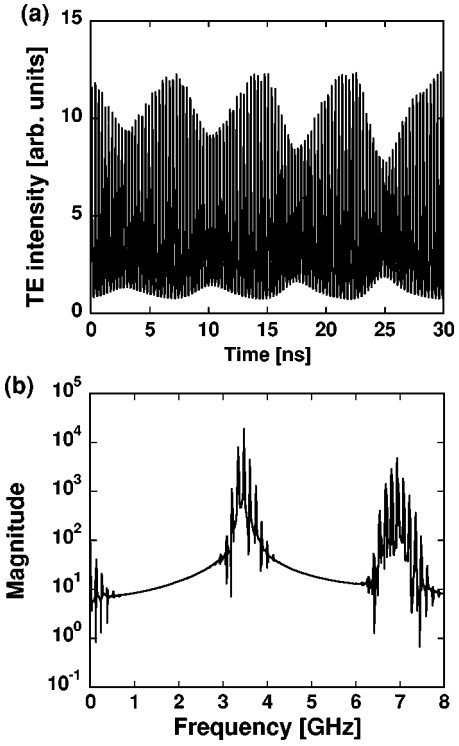

FIG. 8. Numerically calculated intensity dynamics: (a) temporal waveform and (b) the corresponding rf spectrum. The injection current amounts to $J=1.4J_{\mathrm{th,sol}}$.

reduction of the slope of the P-I curve is observed for the total output of the laser with TM-mode feedback, which is consistent with our experimental results shown in Fig. 2.

Next, we investigate the model in regard to features of the temporal waveforms and rf spectra. Figure 8 shows (a) the temporal waveform, and (b) the corresponding rf spectrum for an injection current of $1.4J_{\mathrm{th,sol}}$. The quasiperiodic character of the temporal waveform is in good qualitative agreement with our experimental observation shown in Fig. 3. Accordingly, also the numerically calculated rf spectrum is similar to the experimental results depicted in Fig. 4: the peak value in the spectrum corresponding to the relaxation oscillation frequency increases as the injection current is increased, whereas the interval of the spectral peaks corresponding to the inverse of the propagation time of the external loop remains constant. The amplitude of the temporal waveform is small at small injection currents. As the injection current is increased, the amplitude of the oscillations increases and the quasiperiodic oscillations are observed. Finally, as the injection current is further increased, the amplitude of the waveforms decreases again, and the output is stable over $1.8J_{\mathrm{th,sol}}$.

Figure 9 shows the relationship between the intensities of the TE and TM modes. It is worth noting that the temporal waveform of the TM mode is delayed with respect to that of the TE mode by the propagation time τ of the external feedback loop, showing that the TM mode is following the delayed feedback signal. When the TE mode is fed back to the TM mode, the intensity of the TM mode is changed and acts on the TE mode through the carrier density. This interaction

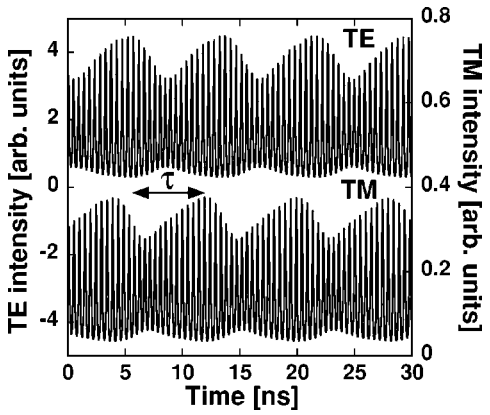

FIG. 9. Temporal waveforms of TE and TM modes at the injection current of $J=1.15J_{\mathrm{th,sol}}$.

between the TE and TM modes through the carrier density is the origin of the oscillation dynamics in this model.

We also observed the relationship between the intensity and phase of the TE mode as shown in Fig. 10. The temporal dynamics of the phase is very similar to the dynamics of intensity, even though there is no term directly coupling the phase and amplitude in Eqs. (3.1) and (3.2). The interaction between the TE- and TM-mode intensities through the carrier density [shown in Eq. (3.5)] generates chaotic instabilities, and the dynamics of both the amplitude and phase are governed by the dynamics of the carrier density, as shown in Eqs. (3.1) and (3.2). Therefore, the phase dynamics are similar to the intensity dynamics. Since the generation of chaotic oscillations is not strongly dependent on the optical phase of the feedback, we can say that the polarization-rotated feedback in our model is a type of ''incoherent'' feedback.

Figure 11 shows the systematic dependence of the dynamics on the injection current using a bifurcation diagram. The bifurcation diagram is created by sampling the peak value of the temporal waveforms as the injection current parameter is changed. In Fig. 11, it is clearly seen that the amplitude of the temporal waveform increases with injection current to a maximum value around the injection current of $1.55J_{\mathrm{th,sol}}$. The output stabilizes around the injection current value of $1.8J_{\mathrm{th,sol}}$. The restabilization of temporal waveforms at high

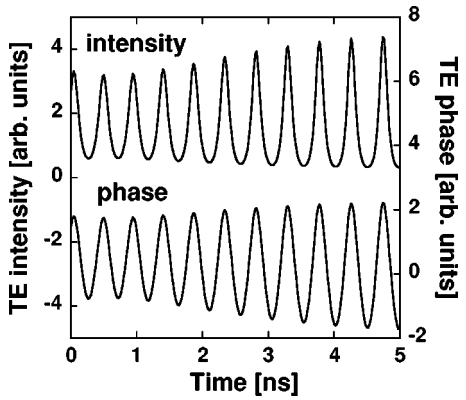

FIG. 10. Intensity and phase dynamics of the TE mode at the injection current of $J=1.15J_{\mathrm{th,sol}}$.

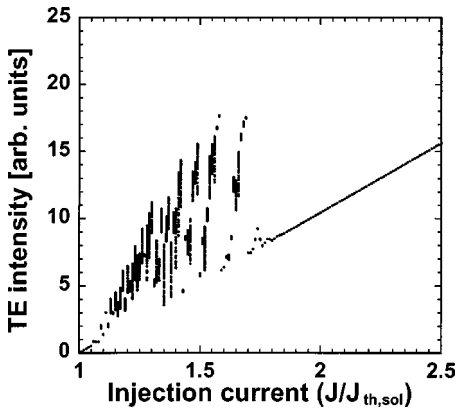

FIG. 11. Bifurcation diagram of the intensity dynamics as a function of the injection current, $J/J_{\mathrm{th,sol}}$.

injection current is an interesting phenomenon. We interpret the mechanism of restabilization as follows. The coupling term of TE and TM modes in Eq. (3.5) needs to be large enough compared with the term for injection current, in order to generate chaotic dynamics. When the injection current is increased, the value of the steady-state solution of the carrier density is increased, and the laser tends to be less sensitive to the feedback light. This restabilization phenomenon is also observed in fully incoherent feedback systems [7–10]. The bifurcation shown in Fig. 11 is consistent with the behavior obtained in our experiments in Fig. 3.

In order to provide an overview of the dependence of the dynamics on the feedback strength, we present another bifurcation diagram for feedback strength in Fig. 12. Figure 12 demonstrates that a large feedback level is required for the onset of self-oscillations, and that the amplitude of the oscillations increases with an increase of the feedback level. These results are also in good qualitative agreement with our experimental observations. We note that the model predicts fully chaotic oscillations for very high feedback levels, which we could not realize in the present experimental setup.

IV. CONCLUSION

In summary, we analyzed the dynamical behavior of a semiconductor laser oscillating mainly in the TE mode sub-

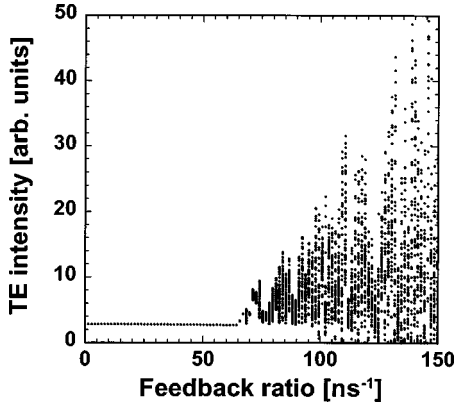

FIG. 12. Bifurcation diagram of the intensity dynamics as a function of the feedback power ratio (injection coefficient, γ_{inj}).

ject to delayed optical feedback injected into the TM mode, and showed the characteristic dependence on the injection current and the feedback level. Comparing our experimental results to previous theoretical studies investigating the concept of incoherent optical feedback, we found similarities concerning the observed dynamics, i.e., quasiperiodic nature of the oscillations obtained for large optical feedback levels and moderate current injection, and the expected absence of a threshold reduction. However, the behavior of the average power, seen in the *P-I* curve, displayed differences. This motivated us to introduce a two-mode rate equation model directly accounting for the delayed optical injection of the dominant TE-mode emission into the TM mode of the laser. Accordingly, the model also includes the TM-mode dynamics of the laser. Numerical simulations using this model show good qualitative agreement with the experiments. In particular, the model matches the observed *P-I* curve and correctly describes the general features of the dynamics in dependence on the feedback level and the injection current. Thus, we have given a comprehensive experimental overview of the dynamics of a semiconductor laser subject to polarization-rotated optical feedback, and presented an alternative theoretical model describing these instabilities. Future work will concentrate on a fuller study of the difference between the TE-TM two-mode model presented in this paper and the conventional incoherent feedback model for a single mode with the carrier density directly modulated by the feedback intensity. On the experimental side, we expect the investigations to focus on schemes for synchronization of the polarization-rotated feedback induced instabilities and the corresponding synchronization behavior. A point of particular interest for practical applications is to find out how sensitively the synchronization of the instabilities depends on the polarization of the light injected into the receiver system.

ACKNOWLEDGMENTS

This research was supported in part by the Telecommunications Advancement Organization of Japan. The authors thank S. Saito and B. Komiyama for their support at ATR. The authors acknowledge fruitful discussions with I. Fischer and W. Elsäßer, F. Rogister, and D. W. Sukow.

[1] L. M. Pecora and T. L. Caroll, Phys. Rev. Lett. **64**, 821 (1990).
[2] G. D. VanWiggeren and R. Roy, Science **279**, 1198 (1998).
[3] G. D. VanWiggeren and R. Roy, Int. J. Bifurcation Chaos Appl. Sci. Eng. **9**, 2129 (2000).
[4] I. Fischer, Y. Liu, and P. Davis, Phys. Rev. A **62**, 011801(R) (2000).
[5] H. Fujino and J. Ohtsubo, Opt. Lett. **25**, 625 (2000).
[6] M. Peil, T. Heil, I. Fischer, and W. Elsäßer, Phys. Rev. Lett. **88**, 174101 (2002).
[7] K. Otsuka and J.-L. Chern, Opt. Lett. **16**, 1759 (1991).
[8] K. Otsuka and J.-L. Chern, Phys. Rev. A **45**, 5052 (1992).
[9] J.-L. Chern, K. Otsuka, and F. Ishiyama, Opt. Commun. **96**, 259 (1993).
[10] F. Ishiyama, J. Opt. Soc. Am. B **16**, 2202 (1999).
[11] F. Rogister, A. Locquet, D. Pieroux, M. Sciamanna, O. Deparis, P. Mégret, and M. Blondel, Opt. Lett. **26**, 1486 (2001).
[12] F. Rogister, D. Pieroux, M. Sciamanna, P. Mégret, and M. Blondel, Opt. Commun. **207**, 295 (2002).
[13] J. M. Saucedo Solorio, D. W. Sukow, D. R. Hicks, and A. Gavrielides, Opt. Commun. **214**, 327 (2002).
[14] H. Yasaka and H. Kawaguchi, Appl. Phys. Lett. **53**, 1360 (1988).
[15] H. Yasaka, Y. Yoshikuni, and H. Kawaguchi, IEEE J. Quantum Electron. **27**, 193 (1991).
[16] J. Houlihan, G. Huyet, and J. G. McInerney, Opt. Commun. **199**, 175 (2001).
[17] I. Fischer, T. Heil, and W. Elsäßer, in *Fundamental Issues of Nonlinear Laser Dynamics*, edited by B. Krauskopf and D. Lenstra, AIP Conf. Proc. No. 548 (AIP, Melville, NY, 2000), p. 218.
[18] A. Uchida, Y. Liu, I. Fischer, P. Davis, and T. Aida, Phys. Rev. A **64**, 023801 (2001).
[19] D. W. Sukow, T. Heil, I. Fischer, A. Gavrielides, A. Hohl-AbiChedid, and W. Elsäßer, Phys. Rev. A **60**, 667 (1999).
[20] G. Huyet, S. Balle, M. Giudici, G. Giacomelli, and J. R. Tredicce, Opt. Commun. **149**, 341 (1998).
[21] S. Tang and J. M. Liu, IEEE J. Quantum Electron. **37**, 329 (2001).
[22] S. Tang and J. M. Liu, Opt. Lett. **26**, 596 (2001).
[23] S. Tang and J. M. Liu, Opt. Lett. **26**, 1843 (2001).
[24] Y. C. Chen and J. M. Liu, Appl. Phys. Lett. **50**, 1406 (1987).
[25] Y. C. Chen and J. M. Liu, Opt. Quantum Electron. **19**, 93 (1987).
[26] S. Ramanujan, G. P. Agrawal, J. M. Chwalek, and H. Winful, IEEE J. Quantum Electron. **32**, 213 (1996).